Shock Compression of a Fifth Period Element: Liquid Xenon to 840 GPa

Seth Root,* Rudolph J. Magyar, John H. Carpenter, David L. Hanson, and Thomas R. Mattsson
Sandia National Laboratories, Albuquerque, New Mexico 87185, USA
(Received 12 April 2010; published 17 August 2010)

Current equation of state (EOS) models for xenon show substantial differences in the Hugoniot above 100 GPa, prompting the need for an improved understanding of xenon's behavior at extreme conditions. We performed shock compression experiments on liquid xenon to determine the Hugoniot up to 840 GPa, using these results to validate density functional theory (DFT) simulations. Despite the nearly fivefold compression, we find that the limiting Thomas-Fermi theory, exact in the high density limit, does not accurately describe the system. Combining the experimental data and DFT calculations, we developed a free-energy-based, multiphase EOS capable of describing xenon over a wide range of pressures and temperatures.

DOI: 10.1103/PhysRevLett.105.085501 PACS numbers: 62.50.Ef, 71.15.Pd, 71.30.+h

Recently, xenon has drawn considerable interest because of its ability to form complex compounds at high pressures [1], its form in Earth's interior [2], and how these characteristics affect the missing xenon problem in Earth's atmosphere [3]. Alongside experimental investigations, density functional theory (DFT)-based [4] methods are increasingly being employed to shed light on the structure of matter under high pressures and high temperatures. The integrated use of shock compression experiments and DFT modeling aimed at understanding the thermophysical behavior of matter under extreme conditions has been instrumental to recent developments in planetary astrophysics and inertial confinement fusion (ICF). For example, shock compression work on carbon has verified the existence of a triple point that carries implications on the use of diamond as an ablator material for ICF capsules [5]. Hugoniot measurements on liquid deuterium [6] were required to validate *ab initio*-based EOS for hydrogen, which largely determines the planetary structure models of gas giants [7,8].

Although DFT methods have been validated to reliably model light elements at extreme conditions [5,7], xenon, with its relativistic core states and *d* electrons, poses additional challenges under pressure, and discrepancies with experimental data exist. In particular, diamond anvil cell work [9] and DFT simulations [10] disagree over the xenon melt curve, a situation similar to the recently explained anomaly in Ta [11]. For xenon an fcc-bcc phase transition was proposed [12], but further experiments are needed to validate the molecular dynamics (MD) predictions. The challenges in modeling xenon are also evident in that current equation of state (EOS) models [13–15] rapidly diverge above 100 GPa on the Hugoniot, creating unacceptable uncertainties at high pressures. Under pressure xenon undergoes an insulator to metal transition [16,17], allowing for direct measurement of the shock front velocity. Thus, xenon Hugoniot states can be determined to high precision and the results used to validate fundamental theoretical methods and models. In this Letter, we measure the liquid xenon Hugoniot to 840 GPa, ~700 GPa higher than previous shock work. The experiments validate the use of DFT-based MD for shock compressed xenon to 500 GPa. Lastly, we use the experimental and DFT results to develop a multiphase EOS.

Shock compression experiments on liquid xenon were performed using the Sandia *Z* accelerator. *Z* is a pulsed power accelerator capable of producing currents and magnetic fields greater than 20 MA and 10 MG. The large current and field densities generate magnetic pressures up to ~650 GPa that can accelerate flyer plates up to 40 km/s [18]. Figure 1 shows a schematic view of the shock experiment. Targets consisted of a copper cell with a 450 μm *Z*-cut, α-quartz front drive plate and 1.5 mm *Z*-cut, α-quartz rear window (single crystals, Argus International). One experiment used an aluminum 6061-T6 drive plate (250 μm) instead of quartz. The sample space (200 μm) was filled with high purity (>99.999%), natural isotope composition, xenon (Matheson Tri-Gas) to 16.5 psi and cooled to 163.5 K [19]. The initial xenon density was calculated from a linear fit of density-temperature data [20] and ranged from 2.965 to 2.972 g/cc with an uncertainty of 0.1%. The initial densities of the quartz and aluminum drive plates at 163.5 K were calculated using SESAME 7360 [21] and 3700 [22], respectively. The flyers were aluminum 6061-T6 with initial thicknesses of 850 or

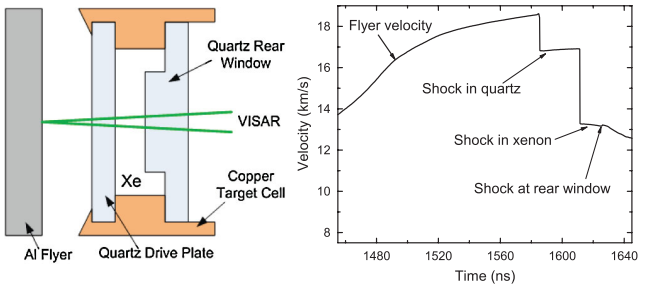

FIG. 1 (color). Left: The *Z* shock compression experiments. Right: Representative VISAR data. Impact and shock transitions are indicated by the sharp changes in the VISAR signal.

1000 μm. A velocity interferometer system for any reflector (VISAR) [23] was used to measure flyer (V_F) and shock (U_S) velocities with an uncertainty of 0.2%–0.5%. Typically, multiple VISAR signals were measured, eliminating 2π phase shift ambiguities and further reducing velocity uncertainties.

Figure 1 shows the VISAR measurement from one experiment. The VISAR tracked the flyer plate velocity up to impact, indicated by the sharp change in the velocity profile. Upon impact, quartz melted into a conductive fluid [24] causing the shock front to be strongly reflective, and allowing for direct measurement of the quartz U_S. The shock transition into the xenon was also reflective, so the xenon U_S was measured directly as well. The particle velocity, pressure, and density (U_P, P, and ρ) were calculated using a Monte Carlo impedance matching (MCIM) method to solve the Rankine-Hugoniot equations [25]. The quartz Hugoniot was modeled with a cubic fit and parameter correlation matrix determined from the quartz data in Ref. [24]. A linear fit and parameter correlation matrix for aluminum were calculated from data in Ref. [26]. In each MCIM calculation, the measured quartz and xenon shock velocities and the initial xenon density were varied about their mean using a random number with standard deviation equal to the measurement uncertainty. Uncertainty in the quartz (or aluminum) Hugoniot was accounted for by varying the fit parameters about their mean using correlated random numbers. The final Hugoniot state was defined as the mean of the MCIM calculation with uncertainty equal to 1 standard deviation. The results are listed in Table I.

In DFT, the accuracy depends on the approximate exchange-correlation functional. We employed two complementary functionals: the local density approximation (LDA) and the Armiento-Mattsson (AM05) [27] functional. LDA is expected to perform accurately in the high density limit, but even in the low density limit the lattice constants and bulk moduli for solid xenon are reasonably accurate. The AM05 functional is designed to capture the effects of inhomogeneity by matching results for electronic edges [27]. In the uniform density limit, the functional approaches LDA. AM05 has demonstrated high fidelity for wide classes of solids [28,29] under normal conditions and was recently validated to 1.6 TPa under shock compression [24]. Importantly for this work, AM05 shows a complete absence of van der Waals (vdW) attraction [29]. In the low density limit, the lack of vdW attraction results in an unstable reference state. This deliberate omission, however, allows for the systematic inclusion of vdW through a modification of the functional or perturbation schemes if necessary. The AM05 functional offers a potentially more accurate description of the repulsive part of the pair interaction between xenon atoms than the LDA, which has been seen to be important in recent work on vdW dimers [30]. Although DFT calculations of closed-shell atoms such as xenon are unreliable at normal conditions, at higher pressures the dispersion of low lying conduction band orbitals reduces the band gap and at high enough pressure results in a transition from an insulating to metallic state. It is expected that a density functional description of this metallic state will be highly accurate, and both functionals used in this study perform well for high-Z transition metals [28,29].

TABLE I. Z experimental and DFT Hugoniot data.

U_P (km/s)		U_s (km/s)		Density (g/cc)	Pressure (GPa)	
9.98 ± 0.03		13.24 ± 0.04		12.09 ± 0.19	392.7 ± 1.5	
11.02 ± 0.03		14.46 ± 0.04		12.48 ± 0.19	472.6 ± 1.6	
11.97 ± 0.05		15.57 ± 0.05		12.83 ± 0.26	552.6 ± 2.7	
13.90 ± 0.04		17.79 ± 0.04		13.58 ± 0.23	733.8 ± 2.9[a]	
14.89 ± 0.05		18.88 ± 0.05		14.07 ± 0.25	835.5 ± 3.1	
LDA	AM05	LDA	AM05		LDA	AM05
1.55	1.56	3.28	3.30	5.64	15.14	15.28
3.21	3.21	5.27	5.26	7.59	50.15	50.10
4.39	4.32	6.63	6.54	8.77	86.43	83.93
5.39	5.29	7.81	7.65	9.58	124.9	119.9
6.15	6.07	8.71	8.59	10.10	159.1	154.7
7.15	7.06	9.88	9.76	10.74	209.7	204.8
7.69	7.56	10.53	10.35	11.00	240.5	232.3
8.42	8.21	11.40	11.11	11.36	284.9	270.8
9.89	9.79	13.19	13.05	11.88	387.3	379.4
11.27	11.10	14.84	14.61	12.35	496.5	481.3[b]

[a]Aluminum drive plate used for this experiment.
[b]Extrapolated from calculations up to 80 kK.

The DFT-MD simulations were performed with VASP 5.1.40 [31,32] using stringent settings [33,34], and convergence tests are documented [35]. Electronic states are occupied according to Mermin's finite-temperature formulation of DFT [36]. All computational details are given in Ref. [35] and the supplementary material [37]. The calculations use liquid xenon at a $\rho_0 = 2.97$ g/cc and $T = 163$ K as the reference state, similar to the experimental initial conditions. The hydrostatic Hugoniot condition is expressed as $2(E - E_{\mathrm{ref}}) = (P + P_{\mathrm{ref}})(v_{\mathrm{ref}} - v)$, with E the internal energy per atom, P the system pressure, and v the volume per atom. E_{ref}, P_{ref}, and v_{ref} are the initial state energy, pressure, and volume. The Hugoniot points were calculated using 32 atom cells (see Ref. [35]) at several temperatures for each density. A typical fully thermalized simulation requires of the order 4000 time steps. The velocity Verlet algorithm was used with a time step ranging from 0.5 to 4 fs depending on temperature. Two factors limit the highest possible temperature accessible through simulations: the number of bands required increases significantly with temperature and the excitations of electrons not included in the valence may become significant. Hugoniot points below 12 g/cc occur at temperatures lower than 80 kK, the limit of our calculations, and are determined via an interpolation of several fixed temperature simulations bracketing the target point for a

given density. The results of both the LDA and AM05 calculations are listed in Table I.

Assuming that the dominant DFT calculation error comes from the reference state, we can use knowledge of the DFT functionals to quantify the variation expected and how this affects the Hugoniot curve. LDA overestimates the attractive contribution [29], and since AM05 effectively contains no vdW, it represents a repulsive limit [29]. Thus, the two functionals are expected to bracket the exact pressure result for the true reference point which has zero pressure. We would not expect any reasonably constructed functionals to give results outside this window. We assessed the reference state energy values by calculating the liquid state heat capacity at constant volume and comparing it to known data.

Figures 2 and 3 show the Z experiment and the DFT results in the U_S-U_P and P-ρ planes. Also shown are the previous experimental data [38–40] and the predicted response from two current EOS models: SESAME 5190 (5190) [13] and LEOS 540 (540L) [14]. A third model XEOS 540 [15] (not shown) is qualitatively similar to 540L above 300 GPa. Figure 3 includes static compression data of solid xenon at room temperature [17] for comparison. Although the highest densities for the statically compressed solid xenon and the shock compressed liquid xenon are similar, the pressure in the shocked xenon is ~4.2 times greater. We find that the DFT results agree well with both static and dynamic compression data over a wide temperature range, supporting the predictions in Ref. [10] of a high melting point akin to the Ta behavior [11]. Furthermore, the experimental results show that current EOS models do not accurately describe the Hugoniot at high pressures. The difference in U_S for these models is small, but it creates large uncertainties in P-ρ. For example, the lowest Z experimental point at $\rho = 12.09$ g/cc has $P = 392.7$ GPa while 540L and 5190 predict pressures of 533.1 and 275.2 GPa at that density. A linear fit ($U_S = C_0 + S_1 U_P$) to all experimental data, excluding the lowest U_P point from Ref. [39], produced the optimized parameters $C_0 = 1.624 \pm 0.029$ and $S_1 = 1.163 \pm 0.005$ with a correlation of -0.7673.

The current EOS models are based on separation of the Helmholtz free-energy into ionic and electronic components. The 540L table used a model which coupled Cowan's ionic model with a Thomas-Fermi (TF) electronic component that has a correction applied to generate the correct binding energy [14]. On the other hand, 5190 included both solid and liquid phases, with the ionic component coming from Debye theory and a hard sphere model [13], respectively. Calculations using a local exchange Thomas-Fermi-Dirac (TFD) code [41] comprised the electronic contribution. At low pressures, both tables include vdW loops in the liquid-vapor coexistence region. However, the 5190 table results are better because it uses the more accurate hard sphere model. At high pressures both tables inaccurately describe the experimental and DFT Hugoniot data (Fig. 3), likely because of the electronic models. The TF and TFD models are known to be asymptotically accurate at very high P-T, with less accuracy at moderate pressures. Interestingly, reproducing

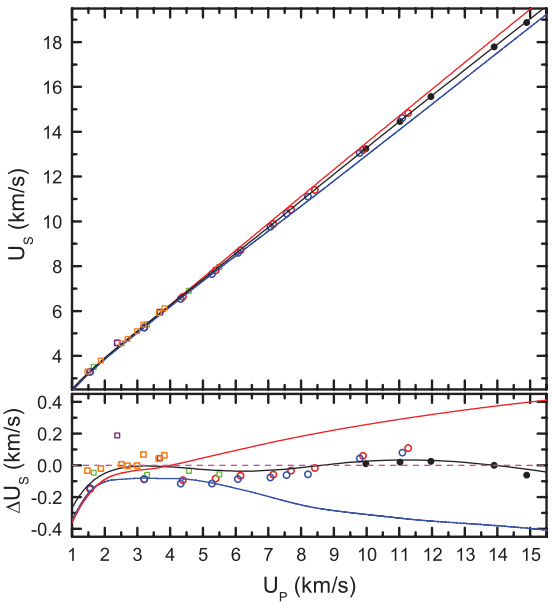

FIG. 2 (color). Top: U_S-U_P Hugoniot plot. Filled black circles, Z data (this work); green square, Ref. [38]; purple square, Ref. [39]; orange square, Ref. [40]; red circle, LDA (this work); blue circle, AM05 (this work); blue line, SESAME 5190; red line, LEOS 540; black line, 5191 (this work). Bottom: Absolute difference from the linear fit to experimental data. Experimental uncertainty is on the order of the data symbol, unless indicated otherwise.

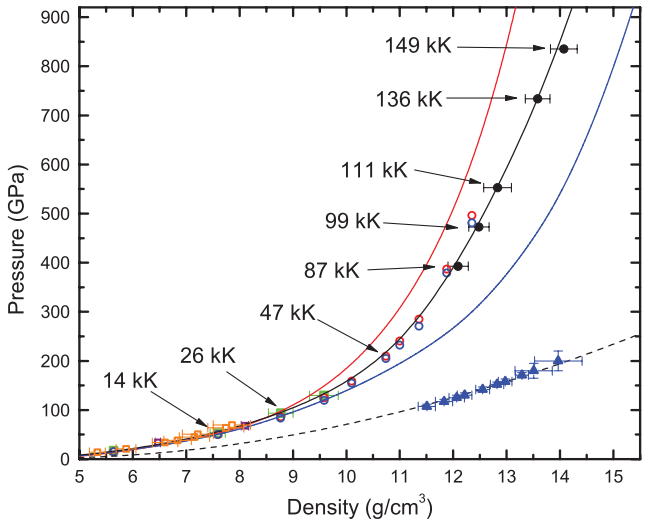

FIG. 3 (color). P-ρ Hugoniot plot. Lines and symbols as in Fig. 2. Black dashed line, 5191 298 K isotherm; blue triangles, solid xenon compression data [17]. Also indicated are Hugoniot temperatures calculated using 5191. Our DFT calculated isotherm [37] agrees with the experimental data [17].

5190, but with nonlocal TFD theory [42], causes the Hugoniot to shift to nearly the same location as 540L, indicating the sensitivity to the electronic component.

With these features in mind, a multiphase EOS was developed that incorporated the Debye and hard sphere models for the ionic component of the solid and liquid phases, along with a general semiempirical electronic model [43] for each phase. This electronic model parametrizes the heat capacity and Grüneisen coefficients that may be calibrated to correct the deficiencies along the Hugoniot while also improving the description of low pressure data. Both models for the new EOS were fit to a variety of experimental data, as well as the DFT calculations of both the isotherm and Hugoniot. A linear U_S-U_P fit biased toward the experimental Hugoniot data above 300 GPa and the DFT Hugoniot below 300 GPa was used to calibrate the EOS parameters. The new EOS was tabulated on a fine grid and is available from the public SESAME library at Los Alamos as table 5191.

We have performed an extensive study of shock compressed liquid xenon up to 840 GPa. Integrating DFT calculations and shock experiments provides a solid basis for understanding the behavior of xenon at extreme pressure over a wide range in temperature. Using these results, we developed a multiphase EOS capable of describing xenon at high pressures and temperatures. These methods are likely applicable to other noble gases.

The authors thank the *Z*-team for contributing to the design, fabrication, and fielding of the experiments. The authors especially appreciate the dedicated efforts of the cryo-team: A. Lopez, J. Lynch, K. Shelton, and R. Smelser. We thank G. Kresse for developing a new xenon projector augmented-wave core potential. Sandia National Laboratories is a multiprogram laboratory managed and operated by Sandia Corporation, a wholly owned subsidiary of Lockheed Martin Corporation, for the U.S. Department of Energy's National Nuclear Securities Administration under Contract No. DE-AC04-94AL85000.

*sroot@sandia.gov

[1] M. Somayazulu *et al.*, Nature Chem. **2**, 50 (2010).
[2] D. Nishio-Hamane *et al.*, Geophys. Res. Lett. **37**, L04302 (2010).
[3] O. R. Pepin, Earth Planet. Sci. Lett. **252**, 1 (2006).
[4] P. Hohenberg and W. Kohn, Phys. Rev. **136**, B864 (1964); W. Kohn and L. J. Sham, Phys. Rev. **140**, A1133 (1965).
[5] M. D. Knudson *et al.*, Science **322**, 1822 (2008).
[6] M. D. Knudson *et al.*, Phys. Rev. Lett. **87**, 225501 (2001).
[7] M. P. Desjarlais, Phys. Rev. B **68**, 064204 (2003).
[8] N. Nettelmann *et al.*, Astrophys. J. **683**, 1217 (2008).
[9] M. Ross *et al.*, Phys. Rev. Lett. **95**, 257801 (2005).
[10] A. B. Belonoshko *et al.*, Phys. Rev. B **74**, 054114 (2006).
[11] A. Dewaele *et al.*, Phys. Rev. Lett. **104**, 255701 (2010).
[12] A. B. Belonoshko *et al.*, Phys. Rev. Lett. **87**, 165505 (2001).
[13] SESAME 5190, in G. I. Kerley and P. M. Henry, Los Alamos National Laboratory Report No. LA-8062, 1980.
[14] LEOS 540 is based on QEOS, R. M. More *et al.*, Phys. Fluids **31**, 3059 (1988).
[15] P. A. Sterne *et al.*, High Energy Density Phys. **3**, 278 (2007).
[16] R. Reichlin *et al.*, Phys. Rev. Lett. **62**, 669 (1989).
[17] K. A. Goettel *et al.*, Phys. Rev. Lett. **62**, 665 (1989).
[18] R. W. Lemke *et al.*, J. Appl. Phys. **98**, 073530 (2005).
[19] D. L. Hanson *et al.*, in *Shock Compression of Condensed Matter 2001*, edited by M. D. Furnish *et al.*, AIP Conf. Proc. No. 620 (AIP, New York, 2001), p. 1141.
[20] A. J. Leadbetter and H. E. Thomas, Trans. Faraday Soc. **61**, 10 (1965).
[21] G. I. Kerley, Kerley Publishing Services, Report No. KPS99-4, 1999.
[22] G. I. Kerley, Int. J. Impact Eng. **5**, 441 (1987).
[23] L. M. Barker and R. E. Hollenbach, J. Appl. Phys. **43**, 4669 (1972).
[24] M. D. Knudson and M. P. Desjarlais, Phys. Rev. Lett. **103**, 225501 (2009).
[25] G. E. Duvall and R. A. Graham, Rev. Mod. Phys. **49**, 523 (1977).
[26] M. D. Knudson *et al.*, J. Appl. Phys. **94**, 4420 (2003).
[27] R. Armiento and A. E. Mattsson, Phys. Rev. B **72**, 085108 (2005).
[28] A. E. Mattsson *et al.*, J. Chem. Phys. **128**, 084714 (2008).
[29] P. Haas *et al.*, Phys. Rev. B **79**, 085104 (2009).
[30] F. O. Kannemann and A. Becke, J. Chem. Theory Comput. **5**, 719 (2009).
[31] P. E. Blöchl, Phys. Rev. B **50**, 17 953 (1994); G. Kresse and D. Joubert, Phys. Rev. B **59**, 1758 (1999).
[32] G. Kresse and J. Hafner, Phys. Rev. B **47**, 558 (1993); Phys. Rev. B **49**, 14 251 (1994); G. Kresse and J. Furthmüller, Phys. Rev. B **54**, 11 169 (1996).
[33] A. E. Mattsson *et al.*, Model. Simul. Mater. Sci. Eng. **13**, R1 (2005).
[34] Projector augmented-wave core potential (Xe_GW 09Jan2009), with 400 eV cutoff.
[35] T. R. Mattsson and R. J. Magyar, in *Shock Compression of Condensed Matter 2009*, edited by M. L. Elert *et al.*, AIP Conf. Proc. No. 1195 (AIP, New York, 2009), pp. 797–800.
[36] N. D. Mermin, Phys. Rev. **137**, A1441 (1965).
[37] See supplementary material at http://link.aps.org/supplemental/10.1103/PhysRevLett.105.085501 for computational details and convergence tests.
[38] W. J. Nellis *et al.*, Phys. Rev. Lett. **48**, 816 (1982).
[39] H. B. Radousky and M. Ross, Phys. Lett. A **129**, 43 (1988).
[40] V. D. Urlin *et al.*, High Press. Res. **8**, 595 (1992).
[41] D. A. Liberman and B. I. Bennett, Group T-4 computer code CANDIDE, Los Alamos National Laboratory, 1980.
[42] R. D. Cowan and J. Ashkin, Phys. Rev. **105**, 144 (1957).
[43] A. V. Bushman *et al.*, *Intense Dynamic Loading Of Condensed Matter* (Taylor & Francis, Washington, DC, 1993).